

Joint Optimization for 4D Human-Scene Reconstruction in the Wild

Zhizheng Liu Joe Lin Wayne Wu Bolei Zhou
University of California, Los Angeles

<https://genforce.github.io/JOSH/>

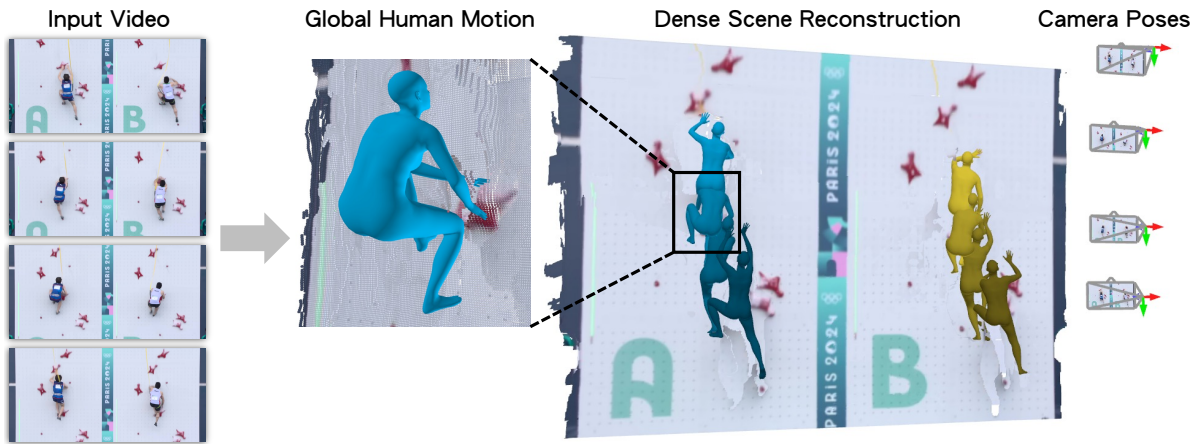


Figure 1. **4D Human-Scene Reconstruction in the wild with JOSH.** Given a web video captured from a single camera, JOSH jointly optimizes the global human motion, the surrounding environment, and the camera poses with coherent human-scene interaction.

Abstract

Reconstructing human motion and its surrounding environment is crucial for understanding human-scene interaction and predicting human movements in the scene. While much progress has been made in capturing human-scene interaction in constrained environments, those prior methods can hardly reconstruct the natural and diverse human motion and scene context from web videos. In this work, we propose JOSH, a novel optimization-based method for 4D human-scene reconstruction in the wild from monocular videos. JOSH uses techniques in both dense scene reconstruction and human mesh recovery as initialization, and then it leverages the human-scene contact constraints to jointly optimize the scene, the camera poses, and the human motion. Experiment results show JOSH achieves better results on both global human motion estimation and dense scene reconstruction by joint optimization of scene geometry and human motion. We further design a more efficient model, JOSH3R, and directly train it with pseudo-labels from web videos. JOSH3R outperforms other optimization-free methods by only training with labels predicted from JOSH, further demonstrating its accuracy and generalization ability.

1. Introduction

Human behaviors and their surrounding environments are closely related to each other, where humans constantly interact with the scene: People sit on benches at plazas, walk through crosswalks at intersections, and use stairs to go upwards on a bridge. Capturing and understanding human-scene interaction is thus crucial to many applications. For example, analyzing how pedestrians navigate crosswalks and sidewalks is essential for the safe deployment of autonomous driving [1]. Meanwhile, designing urban public spaces requires knowing how individuals interact with their surroundings to optimize the group flow, encourage social interaction, and create inviting, accessible environments [2].

Existing research in human-scene interaction mainly focuses on capturing and synthesizing human motion in pre-scanned 3D scenes [3–5]. They first reconstruct the scene without people in constrained environments with complex sensor setups such as multi-view RGBD cameras and laser scanners and then fit the human motion to the environment. Such complex setups limit data accessibility and the capturing of natural and diverse human-scene interactions in the wild. On the other hand, reconstructing global human motion from casual web videos has been a rising topic in

recent years [6, 7]. However, most of the prior works only reconstruct motion without scene context [8–10], and the resulting reconstructed motion lacks grounding and meaning from its surrounding environment.

In this paper, we aim to capture human-scene interactions by tackling monocular 4D human-scene reconstruction, which reconstructs both the 4D global human motion and the 3D scene from web videos. This gives scene-grounding to the reconstructed human motion and makes human-scene interaction data more accessible. A simple baseline to this problem would be combining results from global human motion estimation and monocular dense scene reconstruction. However, such an approach ignores the important interplay between humans and the environment during reconstruction, as the scene context provides physical constraints and goals for human motion. Furthermore, human motion can give functional meaning to the surroundings and help address scale ambiguity in scene reconstruction. Therefore, it is natural and essential to attempt to reconstruct both scenes and humans simultaneously with high accuracy and consistency as 4D human-scene reconstruction.

We propose JOSH (Joint Optimization of Scene Geometry and Human Motion), a novel method for 4D human-scene reconstruction from monocular videos by jointly optimizing the human motion and the scene geometry. As shown in Fig. 1, JOSH can simultaneously reconstruct the dense 3D environment, the camera poses, and the 4D human motion as SMPL [11] body meshes from a single video, producing accurate and coherent human-scene interaction data. JOSH uses techniques in both dense scene reconstruction [12] and human mesh recovery [9] as initialization, and then jointly refines the 4D global human motion and the dense 3D scene point cloud with an optimization process. Our key insight is that human-scene contact can act as strong constraints that bridge the scene and human motion and guide the optimization to produce more accurate and coherent 4D human-scene reconstruction results. To improve the inference speed of JOSH in processing large amounts of video data, we further design an end-to-end model, JOSH3R (JOint Scene and Human 3D Reconstruction), with a lightweight human trajectory head based on a pre-trained 3D scene geometry feature extractor [13] to predict the relative human transformation directly between two frames. JOSH3R can output both dense scene points and human trajectory in a single forward pass, allowing real-time inference as a trade-off to the estimation accuracy.

Experiment results on the EMDB [7], SLOPER4D [14], and RICH [4] datasets demonstrate that JOSH can generate accurate and consistent 4D human-scene reconstruction. Specifically, JOSH sets a new state-of-the-art for global human estimation of EMDB, surpassing previous methods by a large margin. JOSH also produces more accurate camera pose estimation and dense scene reconstruction results than

prior works, highlighting the effectiveness of joint human-scene optimization. We further evaluate JOSH3R on the SLOPER4D dataset, and the results show that JOSH3R can outperform existing optimization-free approaches in human trajectory estimation by training only with labels predicted by JOSH, further showcasing the generalization ability of JOSH on processing noisy web videos.

We summarize our main contribution as follows: 1) A novel method, JOSH, is proposed to tackle the challenge of 4D human-scene reconstruction in the wild by jointly optimizing motion and scene with the human-scene contact constraints. 2) An efficient model variant, JOSH3R, is designed to estimate human-scene reconstruction in real-time, greatly expediting web video processing. 3) Experiment results show that JOSH achieves better accuracy for both global human motion estimation and dense scene reconstruction than other methods, and JOSH3R achieves competitive results by training only with labels predicted by JOSH.

2. Related Work

Monocular Global Human Motion Estimation. Estimating global human motion in the world coordinates from a single monocular video is a challenging task as the camera motion and the human motion are entangled in the video, and we need to recover both motions in metric units. While estimating human motion in the local camera coordinate is straightforward with end-to-end models [15] and large-scale training data [16], how to transform the camera-frame human motion to the global frame still remains an open-ended problem [17, 18]. GLAMR and HuMoR [19, 20] propose to leverage the motion prior from human poses and predict the ego movements between frames, leading to noisy and unreliable predictions, especially for the rare poses. An alternative solution is to estimate the camera motion with SLAM [21] and then transform the camera-coordinate motion to the global coordinate with the estimated camera poses. The key challenge here is to resolve the scale ambiguity of the poses: TRAM [9] proposes to estimate scale from monocular depth estimation, WHAC [22] estimates the scale from the human motion, and OfCam [23] estimates the scale from human mesh depth. SLAHMR [24] proposes an optimization pipeline that jointly optimizes the scale and the human meshes using both the human motion prior and SLAM camera poses. WHAM [8] performs such optimization implicitly with an end-to-end model by taking the SLAM camera angular velocity as input and learning the human motion prior from 3D key points sequences of AMASS [25]. In contrast, COIN [10] learns the motion prior from a diffusion model. Though many methods [8, 9, 24] include a SLAM module in their pipeline, they treat SLAM as a stand-alone module and do not optimize the scene, the human motion, and the camera motion in a single stage. Unlike existing approaches, our method JOSH jointly optimizes both the dense

scene background and the foreground human motion for 4D human-scene reconstruction, and we show that such joint optimization can also benefit the monocular global human estimation task.

Human-Scene Interaction and Reconstruction. Many methods are proposed to capture human-scene interaction data. They set up additional sensors [4, 5, 14] like multi-view RGBD cameras and laser scanners or use multiple shots of the same scene [26] to first get ground-truth 3D labels of the environment, and the human-scene interaction can then be obtained by fitting the SMPL human meshes with the ground-truth scene reconstruction and camera poses [3, 27]. While such an approach can provide accurate results, it is not scalable to casual web videos where both the dense 3D scene and the human motion need to be estimated from a single camera. Other works address reconstructing human-object interactions from monocular videos [28, 29], but they focus more on the interaction with a single object instead of grounding the global human motion in its surrounding scene. To reconstruct the 3D scene from a single camera, traditional approaches [30] use feature matching and bundle adjustment and recent works [13, 21, 31] introduce deep learning into the reconstruction pipeline with more robust performance. Some works also address the more challenging task of 4D scene reconstruction with dynamic objects, where [32] proposes to learn the dynamic scenes with an end-to-end model, and [33] reconstructs the scene with dynamic 4D Gaussians Splatting. These methods aim to reconstruct general dynamic scenes without treating humans separately, while our method JOSH focuses on reconstructing scenes together with the global human motion as fine-grained SMPL meshes. In addition, most prior scene reconstruction methods can only recover the scene geometry up to an unknown scale factor, while JOSH can reconstruct the scene on a metric scale thanks to the joint optimization.

3. Preliminaries

4D human-scene reconstruction involves both global human motion estimation and dense scene reconstruction. We introduce preliminaries of these two tasks in Sec. 3.1 and Sec. 3.2, respectively. We then formalize the task of 4D human-scene reconstruction from monocular videos in Sec. 3.3.

3.1. Global Human Motion Estimation

In global human motion estimation, the goal is to reconstruct the 4D human motion as SMPL human meshes in the world coordinate. The SMPL model takes the parameters $\{\mathbf{T}_g^t, \boldsymbol{\theta}^t, \boldsymbol{\beta}\}_{t=1}^N$ at each timestep and outputs the human body mesh $\mathbf{H}_g^t \in \mathbb{R}^{6890 \times 3}$, where $\boldsymbol{\theta}^t \in \text{SO}(3)^{23}$ is the local orientation of the 23 body joints, $\boldsymbol{\beta} \in \mathbb{R}^{10}$ represents the body shape of the human, and $\mathbf{T}_g^t \in \text{SE}(3)$ is the global transfor-

mation matrix of the SMPL meshes in the world coordinate. To disentangle the camera motion and the human motion, we can decompose $\mathbf{T}_g^t = \mathbf{P}^t \cdot \mathbf{T}_c^t$, where $\mathbf{P}^t \in \text{SE}(3)$ is the camera extrinsics and $\mathbf{T}_c^t \in \text{SE}(3)$ is the transformation matrix of the SMPL meshes in the local camera coordinate. Therefore, an accurate reconstruction of the global human motion depends on a precise estimation of both the camera poses and the local SMPL transformations.

3.2. Dense Scene Reconstruction

In dense scene reconstruction, the goal is to recover the 3D geometry of the environment given by the dense point cloud $\mathbf{X} \in \mathbb{R}^{N \times h \times w \times 3}$. \mathbf{X} consists of the point cloud of each timestep: $\mathbf{X} = \bigcup_{t=1}^N \{\mathbf{X}^t | \mathbf{X}^t = \pi_t^{-1}(\mathbf{K}, \mathbf{P}^t, \sigma^t, \mathbf{Z}^t)\}$, where $\mathbf{K} \in \mathbb{R}^{3 \times 3}$ is the camera intrinsic matrix, $\sigma^t \in \mathbb{R}$ is the scale for each frame, $\mathbf{Z}^t \in \mathbb{R}^{h \times w}$ is the dense depth map for each frame, and $\pi_t^{-1}(\cdot)$ is the unprojection from 2D pixels of frame t to 3D points in the world coordinate given the intrinsics and extrinsics, the scale, and the depth map. JOSH is compatible with all dense scene reconstruction methods that can provide the above parameters. In our implementation, we use MAST3R [13] and MAST3R-SfM [12] for their high efficiency and robustness. Here we provide a brief overview of these works.

MAST3R. Given an image pair I^i, I^j , MAST3R first uses a siamese ViT encoder and twin ViT decoders to get a feature map $\mathbf{F}^i, \mathbf{F}^j$, and then uses separate prediction heads to predict the 3D point cloud $\mathbf{X}^i, \mathbf{X}^j \in \mathbb{R}^{h \times w \times 3}$ in image i 's camera coordinate for local 3D reconstruction and the dense feature maps for pixel-wise matching. The matching result is $\mathbf{C}^{i,j} = \{(\mathbf{x}^i, \mathbf{x}^j, c) | \mathbf{x}^i \in \mathbf{X}^i, \mathbf{x}^j \in \mathbf{X}^j\}$, where \mathbf{x}^i and \mathbf{x}^j are corresponding 3D points, and c is the confidence of their matching from cosine similarity of their matching features.

MAST3R-SfM. MAST3R-SfM proposes to jointly recover camera poses and 3D geometry of a scene given a set of unconstrained images by aligning pair-wise local reconstructions from MAST3R in the world coordinate system. It first constructs a global scene graph $\mathcal{G} = (\mathcal{V}, \mathcal{E})$ and runs MAST3R on each edge in the scene graph. It then calculates an initial prediction of the dense depth map \mathbf{Z} , the camera pose \mathbf{P} , the global scale σ , and the point cloud \mathbf{X} in the world coordinate for each frame by aggregating pair-wise predictions. Next, it uses the point correspondence $\{\mathbf{C}^{i,j} | (i, j) \in \mathcal{E}\}$ to perform global joint optimization of all parameters. The loss includes 3D correspondence loss and 2D reprojection loss as follows:

$$\mathcal{L}_{3D} = \sum_{(\mathbf{x}^i, \mathbf{x}^j, c) \in \mathbf{C}^{i,j}, (i,j) \in \mathcal{E}} c \cdot \rho(\mathbf{x}^i - \mathbf{x}^j) \quad (1)$$

$$\mathcal{L}_{2D} = \sum_{(\mathbf{x}^i, \mathbf{x}^j, c) \in \mathbf{C}^{i,j}, (i,j) \in \mathcal{E}} c \cdot \left[\frac{\rho(\pi_i(\mathbf{x}^i) - \pi_i(\mathbf{x}^j)) + \rho(\pi_j(\mathbf{x}^i) - \pi_j(\mathbf{x}^j))}{\rho(\pi_j(\mathbf{x}^i) - \pi_j(\mathbf{x}^j))} \right] \quad (2)$$

$$\mathcal{L} = w_{3D} \cdot \mathcal{L}_{3D} + w_{2D} \cdot \mathcal{L}_{2D}, \quad (3)$$

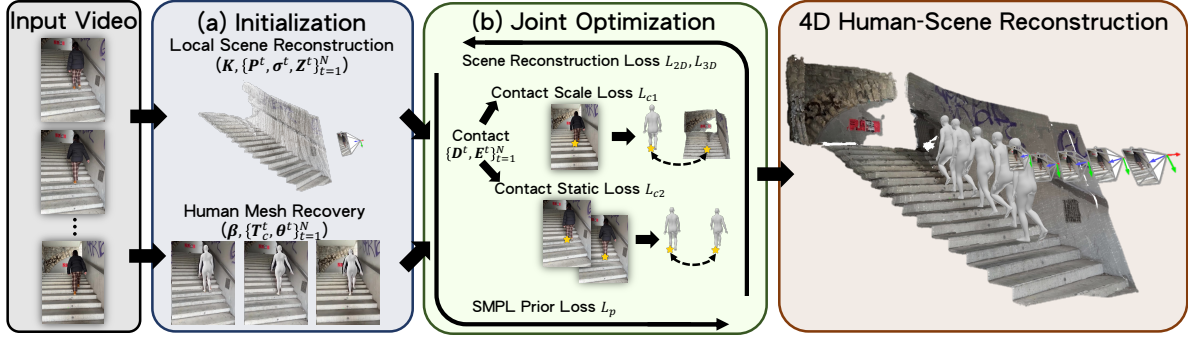


Figure 2. **Overview of JOSH.** Given an input video: (a). JOSH first initializes the local scene reconstruction and local SMPL meshes from pre-trained models. (b). JOSH then jointly optimizes the dense scene point cloud and the global human motion with the human-scene contact losses inferred from the contact labels and the other losses to predict 4D human-scene reconstruction.

where $\pi_i(\cdot)$ projects 3D points in the world coordinate to the pixel locations in frame i , $\rho(\cdot)$ is a robust loss to deal with potential outliers.

3.3. 4D Human-Scene Reconstruction

We aim to tackle the problem of 4D human-scene reconstruction, which reconstructs the global human motion, the surrounding scene context, and the camera parameters from in-the-wild videos. The input is a single monocular video with a sequence of images $\{\mathbf{I}^t \in \mathbb{R}^{h \times w \times 3}\}_{t=1}^N$, where N is the total number of frames. The output contains $(\mathbf{K}, \beta, \{\mathbf{P}^t, \mathbf{T}_c^t, \theta^t, \sigma^t, \mathbf{Z}^t\}_{t=1}^N)$, including the camera intrinsic and extrinsic parameters, the SMPL human mesh parameters, and the dense depth maps with global scales. For notation simplicity, we only consider the case where there is only one person in the scene, but our method also supports reconstructing the motion of multiple people.

4. Joint Optimization of Scene and Human

Existing approaches treat global human motion estimation and dense scene reconstruction as separate tasks, leading to sub-optimal and inconsistent results. To obtain more accurate 4D human-scene reconstruction, we introduce JOSH, a novel method that jointly optimizes the global human motion and the scene geometry, harnessing the contact between the scene and the human body. An overview of JOSH is shown in Fig. 2. We first discuss the initialization before optimization in Sec. 4.1. We then introduce our joint optimization procedure, including the key human-scene contact losses in Sec. 4.2. As JOSH requires iterative optimization, we further propose an optimization-free model JOSH3R for real-time inference in Sec. 4.3.

4.1. Initialization

We first use off-the-shelf models to get an initial value of the parameters for optimization, as shown in Fig. 2 (a).

We use MAST3R [13] to initialize the local scene reconstruction and camera intrinsic and extrinsic parameters. As most dense scene reconstruction methods only work for static environments, dynamic objects like humans in the monocular videos may introduce additional noises in reconstructed point clouds and wrong correspondences, leading to degraded reconstruction performance. Hence, we first segment out the moving foreground objects using a video segmentation model [34], resulting in 2D masks M^i, M^j for each image pair. We then trim the point cloud and the matching results based on the masks, i.e., $\tilde{\mathbf{X}}^i = \{\mathbf{x}^i | \pi_i(\mathbf{x}^i) \in M^i\}$, $\tilde{\mathbf{X}}^j = \{\mathbf{x}^j | \pi_j(\mathbf{x}^j) \in M^j\}$, $\tilde{\mathcal{C}}^{i,j} = \{(\mathbf{x}^i, \mathbf{x}^j, c) | \mathbf{x}^i \in \tilde{\mathbf{X}}^i, \mathbf{x}^j \in \tilde{\mathbf{X}}^j\}$, and proceed with the joint optimization with the trimmed results, which only contain points in the scene background. We also use camera-frame human mesh recovery methods [9, 15] to provide an initial estimation of the local SMPL meshes. As these methods already provide a reliable estimation of the local pose θ^t and shape β parameters, we only optimize the local transformation \mathbf{T}_c^t in the joint optimization. We finally predict the per-vertex contact labels from the image using pre-trained predictors [4], which provides critical human-scene contact information for joint optimization.

4.2. Joint Optimization

Our joint optimization procedure is shown in Fig. 2 (b). Human-scene contact is the key to bridging the separate optimization problems of global human motion estimation and dense scene reconstruction, as it provides contextual constraints and physical grounding. For example, foot-ground contact points help refine foot positioning in motion estimation, ensuring realistic interactions with the environment while improving the accuracy of scene geometry reconstruction. Given the estimated human-scene contact labels, we can infer two important constraints for joint optimization. 1). When the human body and the scene are in contact, they should be close both in the 3D space and in 2D-pixel space

after projection. 2). When a contact is maintained across frames, the contact points should remain static relative to the scene to reduce sliding motion. These constraints can be modeled effectively as contact losses, and our initialization results can provide a dense scene point cloud and detailed SMPL human body meshes for fine-grained optimization.

We first identify the contact correspondences $D^t = \{(\mathbf{x}_h^t, \mathbf{x}_s^t) | \mathbf{x}_h^t \in \mathbf{H}_g^t, \mathbf{x}_s^t \in \tilde{\mathbf{X}}^t\}$, between the vertices of the human body mesh and the 3D points in the scene point cloud for each frame. We start from the predicted contact vertices \mathbf{x}_h^t of the human body mesh in initialization. We require these contact vertices to be visible to avoid depth ambiguities, i.e., $\pi_t(\mathbf{x}_h^t) \in (1 - M^t)$. Next, we search for the corresponding contact point in the scene background with the closest distance to the contact vertex in the pixel coordinate after projecting to the image: $\mathbf{x}_s^t = \operatorname{argmin}_{\mathbf{x}_t \in \tilde{\mathbf{X}}^t} |\pi_t(\mathbf{x}^t) - \pi_t(\mathbf{x}_h^t)|_2$. We empirically find that such a search heuristic generally leads to correct contact correspondences, especially for foot and hand contacts. Finally, we check if the same contact point is maintained in adjacent frames and denote the result as $E^t = \{(\mathbf{x}_h^t, \mathbf{x}_h^{t+1}) | \mathbf{x}_h^t \in \mathbf{H}_g^t, \mathbf{x}_h^{t+1} \in \mathbf{H}_g^{t+1}\}$.

Given the contact correspondences, we can then formulate the two human-scene contact losses:

$$\mathcal{L}_{c1} = \sum_{t \in [1, N], (\mathbf{x}_h^t, \mathbf{x}_s^t) \in D^t} \max(0, |\mathbf{x}_h^t - \mathbf{x}_s^t|_2 - \Delta_{c1}), \quad (4)$$

$$\mathcal{L}_{c2} = \sum_{t \in [1, N-1], (\mathbf{x}_h^t, \mathbf{x}_h^{t+1}) \in E^t} \max(0, |\mathbf{x}_h^t - \mathbf{x}_h^{t+1}|_2 - \Delta_{c2}), \quad (5)$$

where Δ_{c1} and Δ_{c2} are hinge factors. \mathcal{L}_{c1} is the contact scale loss that ensures the corresponding contact points of the human body and the scene background are close in the 3D space, while \mathcal{L}_{c2} is the contact static loss that encourages the same contact points in different frames to remain static in the world coordinate to avoid sliding. We can add the contact losses to the full joint optimization loss as follows:

$$\mathcal{L} = w_{3D} \cdot \mathcal{L}_{3D} + w_{2D} \cdot \mathcal{L}_{2D} + w_{c1} \cdot \mathcal{L}_{c1} + w_{c2} \cdot \mathcal{L}_{c2} + w_p \cdot \mathcal{L}_p, \quad (6)$$

where $\mathcal{L}_p = \sum_{t=1}^N |\mathbf{T}_c^t - \hat{\mathbf{T}}_c^t|_2$ is a SMPL prior loss to make the estimated SMPL local transformations close to their initial values $\hat{\mathbf{T}}_c^t$. \mathcal{L}_{2D} and \mathcal{L}_{3D} are the scene reconstruction losses introduced in Sec. 3.2. We use the loss to optimize all the parameters $(\mathbf{K}, \{\mathbf{P}^t, \mathbf{T}_c^t, \sigma^t, \mathbf{Z}^t\}_{t=1}^N)$ using gradient descent similar to [12]. Note that we do not enforce $\min_t \sigma_t = 1$ to avoid the degenerate solutions as the prior loss \mathcal{L}_p already encodes information about the global scale in metric units.

4.3. End-to-end Prediction with JOSH3R

While JOSH can yield accurate motion estimations, one drawback when processing large amounts of video data is its

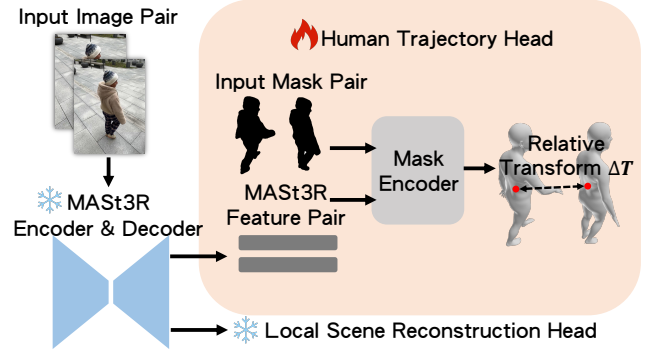


Figure 3. **Architecture of JOSH3R.** Given an input image pair, JOSH3R uses the frozen MASt3R encoder and decoders to obtain the feature map of each image. The human trajectory head then processes the image feature in the mask region with a mask encoder to predict the relative human transformation between the two images.

speed, which is limited by iterative optimization. For some applications, it is desirable to have more efficient processing of large-scale video data as a trade-off to estimation accuracy. We thus design JOSH3R, an end-to-end model variant that jointly infers human trajectory and local scene reconstruction without optimization. Inspired by the strong performance of MASt3R [13] in geometric scene understanding, we introduce a new human trajectory head to output the relative local human transformation ΔT_c^i between adjacent frames, which is in parallel with the original output heads for local scene reconstruction. Assuming the origin of the world coordinate aligns with the camera coordinate of the first frame, the global human transformation and the global camera pose can then be computed iteratively without optimization as:

$$\mathbf{T}_g^t = \prod_{i=1}^{t-1} \Delta T_c^i \cdot \mathbf{T}_c^1, \quad (7)$$

$$\mathbf{P}^t = \mathbf{T}_g^t \cdot (\mathbf{T}_c^t)^{-1}, \quad (8)$$

where \mathbf{T}_c^1 is the local transformation of the SMPL human mesh in the first frame. The architecture of JOSH3R is shown in Fig. 3. The human trajectory head uses the feature maps $\mathbf{F}^i, \mathbf{F}^j$ after the frozen MASt3R encoder and decoder layers, which contain rich information about the geometry of the human’s surrounding environment.

It also takes the human masks M^i, M^j as inputs to encode the human subject’s information. The mask encoder module then encodes the human feature in the masked region, followed by feature pooling to regress the relative transformation ΔT_c^i . More detailed architecture of the human trajectory head can be found in Appendix D.

As all existing datasets for global human mesh recovery are used primarily for evaluation and are small in scale, the lack of training data has become the bottleneck of learning end-to-end global human trajectory models from image in-



Figure 4. **Qualitative 4D human-scene reconstruction results.** a): Qualitative results on the RICH [4] dataset. We compare the ground truth reconstruction with JOSH with joint optimization and the MonST3R* baseline without joint optimization. JOSH has better reconstruction quality and consistency in both global human motion and dense scene reconstruction. b). Qualitative results of web videos. JOSH can reconstruct the motion of multiple people and their surrounding environment in the wild.

puts. To tackle this issue and showcase the generalization ability of JOSH to casual web videos, we propose to train JOSH3R with pseudo-labels annotated by JOSH. We collected a training set containing web videos of pedestrian movements in urban environments and labeled human trajectories in the videos with JOSH. We then train the human trajectory head of JOSH3R with the annotated training data while keeping the other parts of the MAST3R network frozen. We provide more details about the labeling of web videos by JOSH in Appendix B.

5. Experiments

We discuss our experiment setups in Sec. 5.1. We evaluate the global human motion estimation and the dense scene reconstruction performance of JOSH in Sec. 5.2 and Sec. 5.3,

respectively. We analyze the components of JOSH in ablation experiments in Sec. 5.4. Experiments with JOSH3R are presented in Sec. 5.5. Some qualitative results of JOSH for 4D human-scene reconstruction are shown in Fig. 4. The implementation details can be found in Appendix A.

5.1. Experiment Setups

Metrics We separately evaluate the performance of the two sub-tasks of 4D human-scene reconstruction: global human motion estimation and dense scene reconstruction. For global human motion estimation, we use the world-grounded human pose estimation metrics following prior works [8, 9]. We first split sequences into segments of 100 frames and align the predicted human motion in each segment with the ground-truth motion using either the first two frames or the

Table 1. **Global human motion estimation results.** We evaluate on the EMDB [7], SLOPER4D [14], and RICH [4] datasets and compare our method JOSH (bottom row) with state-of-the-art methods in global human motion estimation (top rows) and the baselines from 3D scene reconstruction (middle rows). "Scene" means the method can also provide dense scene reconstruction results.

Methods	Scene	EMDB			SLOPER4D			RICH		
		WA-MPJPE ₁₀₀	W-MPJPE ₁₀₀	RTE%	WA-MPJPE ₁₀₀	W-MPJPE ₁₀₀	RTE%	WA-MPJPE ₁₀₀	W-MPJPE ₁₀₀	RTE%
SLAHMR [24]	✗	326.9	776.1	10.2	706.9	3401.0	12.6	132.2	237.1	6.4
WHAM [8]	✗	131.1	335.3	4.1	297.7	1272.3	10.5	108.4	196.1	4.5
TRAM [9]	✗	76.4	222.4	1.4	816.5	4157.5	17.1	127.8	238.0	6.0
MASt3R* [13]	✓	89.3	252.4	1.8	314.3	1361.4	4.7	115.8	193.9	7.5
MonST3R* [32]	✓	111.6	320.3	3.1	235.6	1005.3	3.1	219.7	384.4	13.6
JOSH (ours)	✓	68.9	174.7	1.3	120.0	438.3	1.8	89.0	132.5	3.0

entire segment. We then compute the mean-per-joint-error in millimeters between the prediction and the ground truth to obtain W-MPJPE₁₀₀ or WA-MPJPE₁₀₀ for evaluation. We also evaluate the global trajectory errors normalized by the total distance after aligning the whole trajectory and measure Root Translation Error (RTE%).

For dense scene reconstruction, as JOSH can reconstruct the scene on a metric scale, we directly compare the prediction and the ground truth without scale alignment. We first evaluate the video depth estimation using absolute relative error (AbsRel) and the fraction of inlier points ($\delta < 1.25$) as well as the camera poses using absolute trajectory error (ATE) in meters as indirect metrics. We then evaluate the dense reconstruction with chamfer distance (CD) in meters, which measures the distance between the predicted point cloud and the ground truth point cloud.

Baselines As no method directly supports 4D human-scene reconstruction, we build the following baselines from recent global human motion estimation and dense scene reconstruction methods for better comparison. All baselines reconstruct human motion and scene separately without joint optimization: 1). **TRAM***: TRAM [9] is the state-of-the-art method for global human motion estimation, and it also provides monocular depth estimation results from ZoeDepth [35] and metric-scale camera poses from masked DROID-SLAM [21]. We combine them to obtain the dense scene reconstruction. 2). **MASt3R***: MASt3R [12] is the state-of-the-art method for monocular dense scene reconstruction, and it already predicts the 3D points on a metric scale. Therefore, we directly use the scene reconstruction and camera poses from MASt3R-SfM [12] and combine the results with the camera-frame human mesh recovery [9] to get the global human motion. 3). **MonST3R***: MonST3R [32] can directly reconstruct dynamic scenes, but its output is scale-ambiguous. We first get the per-frame scale by dividing the depth of the human center from the SMPL mesh by the human depth from the predicted dense depth map. We then estimate the global scale as the median of all per-frame scales and apply it to the predicted depth maps and camera poses to obtain the

metric-scale results and combine them with camera-frame human mesh recovery similar to MASt3R*.

Datasets We evaluate on the following datasets: EMDB [7], SLOPER4D [14], and RICH [4]. All datasets contain dynamic human motions in different environments shot by a moving camera to mimic the in-the-wild setting. The EMDB dataset only provides labels of the global human motion and camera poses without the scene labels, and we use the EMDB-2 subset with 25 sequences for evaluation following previous works [8, 9]. The SLOPER4D dataset has ground truth labels for both the global human motion and the scene annotated from point clouds captured by a LiDAR. It is recorded in urban environments, and we only evaluate the 6 publicly released sequences. The RICH dataset also provides global human motion labels and pre-captured scene meshes from a laser scanner. As only certain sequences of RICH have a video captured by a moving camera without intrinsic and extrinsic parameters, we only use the subset with 40 sequences for evaluation.

5.2. Global Human Motion Estimation

Table 1 shows evaluation results of global human estimation on the EMDB, SLOPER4D, and RICH datasets. On all datasets, JOSH outperforms all prior works in global human motion estimation by a large margin. Specifically, it sets up a new state-of-the-art performance on the most commonly used EMDB dataset with a 68.9 WA-MPJPE₁₀₀ and a 174.7 W-MPJPE₁₀₀. It also achieves a significant 2-3 times less error than the best-performing prior method WHAM [8] on the more challenging SLOPER4D dataset with longer trajectories and more complex backgrounds. JOSH also surpasses all the other baselines that reconstruct both the human motion and the scene geometry. Surprisingly, many of these baseline results for joint reconstruction still achieve on-par or better performance with prior methods that only focus on predicting human motion without jointly reconstructing the scene; this fully demonstrates the necessity to consider human-scene interaction while estimating the global human

Table 2. **Metric-scale scene reconstruction results.** We evaluate on the EMDB [7], SLOPER4D [14], and RICH [4] datasets and compare with the other scene reconstruction baselines.

Methods	EMDB	SLOPER4D				RICH
	ATE ↓	ATE ↓	Abs Rel ↓	$\delta < 1.25$ ↑	CD ↓	CD ↓
TRAM* [9]	1.13	124.8	0.33	0.38	59.70	4.77
MASt3R* [13]	1.51	28.0	0.48	0.07	29.64	3.96
MonST3R* [32]	2.51	20.8	0.25	0.70	10.21	5.43
JOSH (ours)	1.13	7.4	0.18	0.86	7.38	2.81

motion and the effectiveness of our joint optimization in further improving the accuracy.

5.3. Dense Scene Reconstruction

We compare with the other baselines on metric-scale scene reconstruction in Tab. 2. As different datasets contain different labels for evaluating scene reconstruction performance, we only evaluate the available metrics for each dataset. JOSH achieves the same best performance on global camera trajectory estimation on EMDB as TRAM* with an ATE of 1.13. However, as TRAM* directly combines outputs of monocular depth estimation and SLAM camera poses without joint optimization, its performance is not robust and gets a much larger error on the more challenging SLOPER4D dataset. On the other datasets, JOSH also outperforms the baselines in all metrics, including video depth estimation and dense scene reconstruction, highlighting its strong generalization and robustness. As JOSH uses MASt3R as its initialization for dense scene reconstruction, the comparison with MASt3R* clearly shows that jointly optimizing human motion and scene geometry can lead to more accurate scene reconstruction than only optimizing with the scene reconstruction losses. The comparison with MonST3R* also demonstrates that while directly learning the scene dynamics from data is more generalizable, modeling human motion with fine-grained SMPL human meshes and optimizing the background scene with detailed human-scene contact constraints can lead to better reconstruction quality. Some qualitative comparisons are shown in Fig. 5.

5.4. Ablation Studies

We conduct ablation studies on JOSH in Tab. 3 to analyze the benefits of each of our method’s components. Row 1 shows the results without joint optimization by simply combining the scene reconstruction results from [12] and human mesh recovery results from [9]. In Row 2, we add the contact scale loss \mathcal{L}_{c1} to enforce consistency between the scene contact point and human contact point and only optimize the scene reconstruction. The results show significant improvements in dense scene reconstruction, as contact points are used as guidance toward the true scale of the camera poses and the depth maps. We also observe a huge boost in global

Table 3. **Ablation experiments of JOSH on SLOPER4D.** We start with no optimization (Row 1), then add contact scale loss \mathcal{L}_{c1} and only optimize the scene reconstruction (Row 2), add human to the optimization and jointly optimize scene and motion (Row 3), add contact static loss \mathcal{L}_{c2} (Row 4), and add hinge factors to the contact losses to obtain our final method JOSH (Row 5).

Variants	SLOPER4D				
	WA-MPJPE ₁₀₀	W-MPJPE ₁₀₀	RTE%	Abs Rel	ATE
w/o opt	314.3	1361.4	4.73	0.48	28.04
+ \mathcal{L}_{c1} , opt scene	148.9	486.4	1.82	0.18	7.45
+ opt human	121.2	439.9	1.83	0.18	7.43
+ \mathcal{L}_{c2}	120.0	438.8	1.82	0.18	7.40
JOSH	120.0	438.3	1.81	0.18	7.38

Table 4. **Performance analysis of JOSH3R.** We compare the efficiency and accuracy of JOSH3R with the other methods on SLOPER4D. "Opt." means the method includes a post-optimization procedure. "FPS" indicates the amortized frames per second to run inference with all modules of the method. All methods are tested on a Nvidia RTX4090 GPU. For each metric, we bold the result of the best method and underline the result of the second-best method.

Methods	Opt.	FPS	SLOPER4D			
			WA-MPJPE ₁₀₀	W-MPJPE ₁₀₀	RTE%	ATE
SLAHMR [24]	✓	0.1	706.9	3401.0	12.6	65.2
JOSH	✓	0.8	148.6	493.8	1.8	7.4
WHAM [8]	✗	<u>4.4</u>	297.7	1272.3	10.5	58.5
TRAM* [9]	✗	1.1	816.5	4157.5	17.1	124.8
JOSH3R	✗	15.4	<u>271.1</u>	<u>1217.1</u>	<u>10.0</u>	<u>56.1</u>

human motion estimation performance even without optimizing the local SMPL transformations as it also depends on the accuracy of the camera poses. In Row 3, we add local SMPL transformations to the optimization and observe another significant improvement in global human motion estimation, indicating the effectiveness of joint optimization to enhance the accuracy of both scene and motion reconstruction. In Row 4, we see that employing a contact static loss \mathcal{L}_{c2} on contact points can further refine reconstruction quality by reducing motion sliding and jittering. Our final method JOSH in Row 5 shows that adding hinge factors can lead to smoother optimization with better results.

5.5. Experiments with JOSH3R

To analyze the trade-off between the accuracy and efficiency of JOSH3R, we conduct experiments in Tab. 4. Since JOSH3R takes a data-driven approach, we evaluate it on the SLOPER4D dataset as its human motion is similar to the pedestrian movements in urban environments used to train JOSH3R. We can observe that JOSH3R is significantly faster than JOSH, with a 15.4 FPS, allowing real-time inference. Still, JOSH3R performs better and is faster than the other optimization-free methods in both global human motion estimation and camera pose estimation. We want to

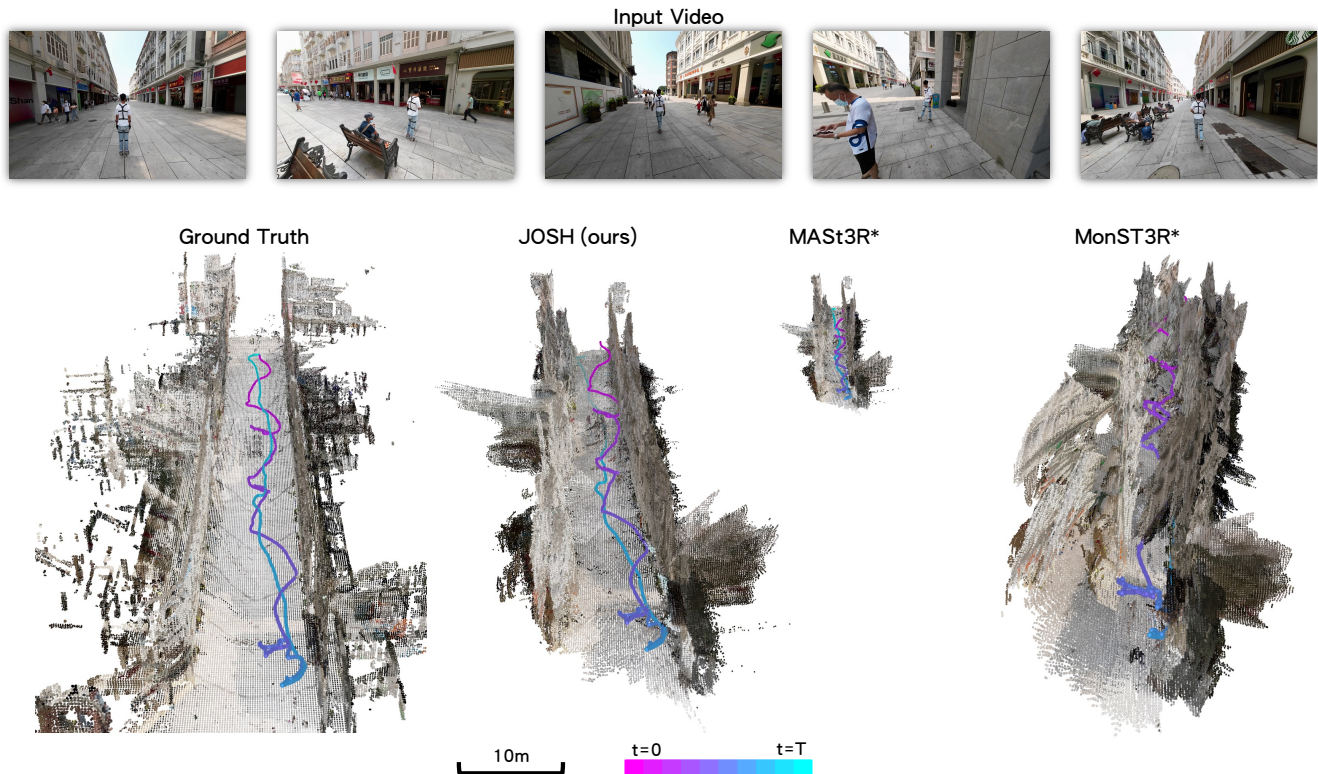


Figure 5. **Qualitative comparisons for large-scale dense scene reconstruction.** We use ‘seq003’ from the SLOPER4D dataset with 6495 frames and a looping camera trajectory. We visualize the reconstructed dense scene point cloud and the camera trajectory on a metric scale. JOSH has the best accuracy compared to the other baselines, while the MASt3R* has the wrong global scale and MonST3R* fails to produce a consistent reconstruction.

stress that JOSH3R is trained only with pseudo labels of web videos annotated by JOSH. This demonstrates both the generalization ability and robustness of JOSH to web videos and the high potential of learning an end-to-end global human motion model from image inputs without post-optimization or SLAM camera poses. We believe the performance of JOSH3R can be further improved with more diverse data and high-quality labels, and we will leave it to future work. We conduct ablation studies on JOSH3R in Appendix D.

6. Conclusion

We present JOSH, a novel method for 4D human-scene reconstruction in the wild. JOSH leverages the human-scene contact to jointly optimize the global human motion as SMPL meshes and scene geometry as dense scene point clouds. The results show that the joint optimization of JOSH can not only produce coherent human-scene interaction data but also achieve better performance in both global human motion estimation and dense scene reconstruction. We believe JOSH could serve as a useful annotation tool to study human-scene interaction for in-the-wild settings with more natural motion and diverse environments.

Limitations. JOSH uses results from other models as initialization, which could suffer from bad initializations even after joint optimization. In addition, JOSH works best when both the contact points on the human and the scene are visible in the 2D image, which could fail in some more challenging settings when the contact correspondences are hard to obtain or there is no contact between the human and the scene.

References

- [1] C. G. Keller and D. M. Gavrila, “Will the pedestrian cross? a study on pedestrian path prediction,” *IEEE Transactions on Intelligent Transportation Systems*, vol. 15, no. 2, pp. 494–506, 2013. 1
- [2] J. Gehl, *Cities for people*. Island press, 2013. 1
- [3] M. Hassan, V. Choutas, D. Tzionas, and M. J. Black, “Resolving 3d human pose ambiguities with 3d scene constraints,” in *Proceedings of the IEEE/CVF international conference on computer vision*, pp. 2282–2292, 2019. 1, 3
- [4] C.-H. P. Huang, H. Yi, M. Höschle, M. Safroshkin, T. Alexiadis, S. Polikovsky, D. Scharstein, and M. J. Black, “Capturing and inferring dense full-body human-scene contact,” in *Proceedings of the IEEE/CVF Conference on Computer Vision and Pattern Recognition*, pp. 13274–13285, 2022. 2, 3, 4, 6, 7, 8, 1
- [5] N. Jiang, Z. Zhang, H. Li, X. Ma, Z. Wang, Y. Chen, T. Liu, Y. Zhu, and S. Huang, “Scaling up dynamic human-scene interaction modeling,” in *Proceedings of the IEEE/CVF Conference on Computer Vision and Pattern Recognition*, pp. 1737–1747, 2024. 1, 3
- [6] T. Von Marcard, R. Henschel, M. J. Black, B. Rosenhahn, and G. Pons-Moll, “Recovering accurate 3d human pose in the wild using imus and a moving camera,” in *Proceedings of the European conference on computer vision (ECCV)*, pp. 601–617, 2018. 2
- [7] M. Kaufmann, J. Song, C. Guo, K. Shen, T. Jiang, C. Tang, J. J. Zárate, and O. Hilliges, “Emdb: The electromagnetic database of global 3d human pose and shape in the wild,” in *Proceedings of the IEEE/CVF International Conference on Computer Vision*, pp. 14632–14643, 2023. 2, 7, 8, 1
- [8] S. Shin, J. Kim, E. Halilaj, and M. J. Black, “Wham: Reconstructing world-grounded humans with accurate 3d motion,” in *Proceedings of the IEEE/CVF Conference on Computer Vision and Pattern Recognition*, pp. 2070–2080, 2024. 2, 6, 7, 8, 1
- [9] Y. Wang, Z. Wang, L. Liu, and K. Daniilidis, “Tram: Global trajectory and motion of 3d humans from in-the-wild videos,” *arXiv preprint arXiv:2403.17346*, 2024. 2, 4, 6, 7, 8, 1
- [10] J. Li, Y. Yuan, D. Rempe, H. Zhang, P. Molchanov, C. Lu, J. Kautz, and U. Iqbal, “Coin: Control-inpainting diffusion prior for human and camera motion estimation,” *arXiv preprint arXiv:2408.16426*, 2024. 2, 1
- [11] M. Loper, N. Mahmood, J. Romero, G. Pons-Moll, and M. J. Black, “Smpl: A skinned multi-person linear model,” in *Seminal Graphics Papers: Pushing the Boundaries, Volume 2*, pp. 851–866, 2023. 2
- [12] B. Duisterhof, L. Zust, P. Weinzaepfel, V. Leroy, Y. Cabon, and J. Revaud, “Mast3r-sfm: a fully-integrated solution for unconstrained structure-from-motion,” 2024. 2, 3, 5, 7, 8, 1
- [13] V. Leroy, Y. Cabon, and J. Revaud, “Grounding image matching in 3d with mast3r,” *arXiv preprint arXiv:2406.09756*, 2024. 2, 3, 4, 5, 7, 8
- [14] Y. Dai, Y. Lin, X. Lin, C. Wen, L. Xu, H. Yi, S. Shen, Y. Ma, and C. Wang, “Sloper4d: A scene-aware dataset for global 4d human pose estimation in urban environments,” in *Proceedings of the IEEE/CVF Conference on Computer Vision and Pattern Recognition (CVPR)*, pp. 682–692, June 2023. 2, 3, 7, 8, 1
- [15] S. Goel, G. Pavlakos, J. Rajasegaran, A. Kanazawa, and J. Malik, “Humans in 4d: Reconstructing and tracking humans with transformers,” in *Proceedings of the IEEE/CVF International Conference on Computer Vision*, pp. 14783–14794, 2023. 2, 4
- [16] M. J. Black, P. Patel, J. Tesch, and J. Yang, “Bedlam: A synthetic dataset of bodies exhibiting detailed lifelike animated motion,” in *Proceedings of the IEEE/CVF Conference on Computer Vision and Pattern Recognition*, pp. 8726–8737, 2023. 2
- [17] M. Kocabas, Y. Yuan, P. Molchanov, Y. Guo, M. J. Black, O. Hilliges, J. Kautz, and U. Iqbal, “Pace: Human and camera motion estimation from in-the-wild videos,” in *2024 International Conference on 3D Vision (3DV)*, pp. 397–408, IEEE, 2024. 2
- [18] Z. Shen, H. Pi, Y. Xia, Z. Cen, S. Peng, Z. Hu, H. Bao, R. Hu, and X. Zhou, “World-grounded human motion recovery via gravity-view coordinates,” in *SIGGRAPH Asia Conference Proceedings*, 2024. 2, 1
- [19] D. Rempe, T. Birdal, A. Hertzmann, J. Yang, S. Sridhar, and L. J. Guibas, “Humor: 3d human motion model for robust pose estimation,” in *Proceedings of the IEEE/CVF international conference on computer vision*, pp. 11488–11499, 2021. 2
- [20] Y. Yuan, U. Iqbal, P. Molchanov, K. Kitani, and J. Kautz, “Glamr: Global occlusion-aware human mesh recovery with dynamic cameras,” in *Proceedings of the IEEE/CVF conference on computer vision and pattern recognition*, pp. 11038–11049, 2022. 2, 1
- [21] Z. Teed and J. Deng, “Droid-slam: Deep visual slam for monocular, stereo, and rgb-d cameras,” *Advances in neural information processing systems*, vol. 34, pp. 16558–16569, 2021. 2, 3, 7
- [22] W. Yin, Z. Cai, R. Wang, F. Wang, C. Wei, H. Mei, W. Xiao, Z. Yang, Q. Sun, A. Yamashita, *et al.*, “Whac: World-grounded humans and cameras,” *arXiv preprint arXiv:2403.12959*, 2024. 2, 1
- [23] F. Yang, K. Gu, H. L. Nguyen, and A. Yao, “Ofcam: Global human mesh recovery via optimization-free camera motion scale calibration,” *arXiv preprint arXiv:2407.00574*, 2024. 2, 1
- [24] V. Ye, G. Pavlakos, J. Malik, and A. Kanazawa, “Decoupling human and camera motion from videos in the wild,” in *Proceedings of the IEEE/CVF conference on computer vision and pattern recognition*, pp. 21222–21232, 2023. 2, 7, 8, 1
- [25] N. Mahmood, N. Ghorbani, N. F. Troje, G. Pons-Moll, and M. J. Black, “Amass: Archive of motion capture as surface shapes,” in *Proceedings of the IEEE/CVF international conference on computer vision*, pp. 5442–5451, 2019. 2
- [26] G. Pavlakos, E. Weber, M. Tancik, and A. Kanazawa, “The one where they reconstructed 3d humans and environments in tv shows,” in *European Conference on Computer Vision*, pp. 732–749, Springer, 2022. 3
- [27] S. Zhang, Y. Zhang, F. Bogo, M. Pollefeys, and S. Tang, “Learning motion priors for 4d human body capture in 3d

- scenes,” in *Proceedings of the IEEE/CVF International Conference on Computer Vision*, pp. 11343–11353, 2021. 3
- [28] C. Huo, Y. Shi, and J. Wang, “Monocular human-object reconstruction in the wild,” in *Proceedings of the 32nd ACM International Conference on Multimedia*, pp. 5547–5555, 2024. 3
- [29] X. Xie, B. L. Bhatnagar, and G. Pons-Moll, “Visibility aware human-object interaction tracking from single rgb camera,” in *Proceedings of the IEEE/CVF Conference on Computer Vision and Pattern Recognition*, pp. 4757–4768, 2023. 3
- [30] J. L. Schonberger and J.-M. Frahm, “Structure-from-motion revisited,” in *Proceedings of the IEEE conference on computer vision and pattern recognition*, pp. 4104–4113, 2016. 3
- [31] S. Wang, V. Leroy, Y. Cabon, B. Chidlovskii, and J. Revaud, “Dust3r: Geometric 3d vision made easy,” in *Proceedings of the IEEE/CVF Conference on Computer Vision and Pattern Recognition*, pp. 20697–20709, 2024. 3
- [32] J. Zhang, C. Herrmann, J. Hur, V. Jampani, T. Darrell, F. Cole, D. Sun, and M.-H. Yang, “Monst3r: A simple approach for estimating geometry in the presence of motion,” *arXiv preprint arxiv:2410.03825*, 2024. 3, 7, 8
- [33] G. Wu, T. Yi, J. Fang, L. Xie, X. Zhang, W. Wei, W. Liu, Q. Tian, and X. Wang, “4d gaussian splatting for real-time dynamic scene rendering,” in *Proceedings of the IEEE/CVF Conference on Computer Vision and Pattern Recognition*, pp. 20310–20320, 2024. 3
- [34] H. K. Cheng, S. W. Oh, B. Price, A. Schwing, and J.-Y. Lee, “Tracking anything with decoupled video segmentation,” in *ICCV*, 2023. 4, 1, 2
- [35] S. F. Bhat, R. Birkl, D. Wofk, P. Wonka, and M. Müller, “Zoedepth: Zero-shot transfer by combining relative and metric depth,” *arXiv preprint arXiv:2302.12288*, 2023. 7
- [36] D. P. Kingma, “Adam: A method for stochastic optimization,” *arXiv preprint arXiv:1412.6980*, 2014. 1
- [37] Z. Cai, W. Yin, A. Zeng, C. Wei, Q. Sun, W. Yanjun, H. E. Pang, H. Mei, M. Zhang, L. Zhang, C. C. Loy, L. Yang, and Z. Liu, “SMPLer-X: Scaling up expressive human pose and shape estimation,” in *Advances in Neural Information Processing Systems*, 2023. 1, 2
- [38] D. Sczepansky, “Poptravel.” <https://www.youtube.com/@poptravelorg>, 2024. Accessed: 2024-11-13. Licensed under CC BY. 1
- [39] Y. Li, H. Mao, R. Girshick, and K. He, “Exploring plain vision transformer backbones for object detection,” in *European conference on computer vision*, pp. 280–296, Springer, 2022. 1
- [40] Y. Sun, Q. Bao, W. Liu, T. Mei, and M. J. Black, “Trace: 5d temporal regression of avatars with dynamic cameras in 3d environments,” in *Proceedings of the IEEE/CVF Conference on Computer Vision and Pattern Recognition*, pp. 8856–8866, 2023. 1

Joint Optimization for 4D Human-Scene Reconstruction in the Wild

Supplementary Material

We provide implementation details of JOSH and JOSH3R in Sec. A. We then discuss the procedure to label web videos using JOSH for training JOSH3R in Sec. B. As EMDB [7] is the most commonly used dataset for global human motion estimation, we compare JOSH and JOSH3R with all the other state-of-the-art methods on EMDB in Sec. C. An ablation study on the model components of JOSH3R is shown in Sec. D.

A. Implementation Details

JOSH We follow [12] to optimize the total loss \mathcal{L} in two stages. The first stage performs coarse alignment by setting $w_{2D} = 0$ and only optimizes the global scale σ^t , the camera pose P^t , and the local SMPL transformation T_c^t . The second stage further refines the results with the 2D projection loss by setting $w_{2D} = 0$ and optimizes all the parameters. The other loss weights are set to be $w_{e1} = 1, w_{e2} = 20, w_p = 10$. Hinge factors for \mathcal{L}_{c1} and \mathcal{L}_{c2} are 0 and 0.1, respectively. Both stages are optimized with Adam [36], and the learning rate is set to 0.07 and 0.014 in the two stages, with the number of iterations set to 500 and 200, respectively. We use VIMO [9], a state-of-the-art model for camera-frame human motion estimation from a video to initialize the SMPL parameters before joint optimization, and BSTRO [4] for estimating the per-vertex contact labels. As it is slow and computationally expensive to optimize the entire long sequence, we split each sequence into segments of 100 frames to perform local reconstruction and concatenate the results afterward. We sample the keyframe every 0.2s and interpolate the camera poses in between. Note that to optimize scenes with multiple humans, we simply add supplemental prior losses \mathcal{L}_p and contact losses L_{c1}, L_{c2} for each additional person, as shown below:

$$\mathcal{L} = \mathcal{L}_{3D} + \mathcal{L}_{2D} + \sum_{i=1}^O (\mathcal{L}_{c1,i} + \mathcal{L}_{c2,i} + \mathcal{L}_{p,i}), \quad (9)$$

where O is the number of people.

JOSH3R We train JOSH3R for 50 epochs on in-the-wild videos annotated by JOSH. The learning rate is set to $1e-4$ with a batch size of 64 on 8 Nvidia RTX A6000 GPUs. Due to limited training data, we sample image pairs with temporal intervals between 1-10 frames during training and also apply data augmentations, including random cropping, flipping, rotation, and color jittering so that the model can generalize better to different camera fps, intrinsics, and movements. During inference, the image pairs are sampled every 0.2s, and we also interpolate the human trajectories in between. We combine the human trajectory from JOSH3R with the local SMPL meshes predicted by SMPLer-X [37] to get the complete global human motion.

B. Labeling Web Videos with JOSH

We collect 13 full-length web videos of pedestrians walking in cities worldwide posted by content creators on YouTube [38] with

Methods	EMDB		
	WA-MPJPE ₁₀₀	W-MPJPE ₁₀₀	RTE%
TRACE [40]	529.0	1702.3	17.7
GLAMR [20]	280.8	726.6	11.4
SLAHMR [24]	326.9	776.1	10.2
WHAM [8]	131.1	335.3	4.1
WHAC [22]	142.2	389.4	-
OfCaM [23]	108.2	317.9	2.2
COIN [10]	152.8	407.3	3.5
GVHMR [18]	109.1	274.9	1.9
TRAM [9]	76.4	222.4	1.4
JOSH3R (ours)	<u>220.0</u>	<u>661.7</u>	<u>13.1</u>
JOSH (ours)	68.9	174.7	1.3

Table 5. Global human motion estimation results on EMDB.

diverse pedestrian movements and scene backgrounds. All videos have a Creative Commons license and we remove all personally identifiable information when processing them. We split each video into 5-second clips (150 frames) and collected 3175 video clips. To annotate the human trajectory, we first use VitDet [39] to detect and DEVA [34] to track the pedestrians and run JOSH to jointly optimize the trajectories of all pedestrians and the scene background in each video clip. In total, we collect about 460,000 frames of global human motion pseudo-labels. Note that though we only use 13 videos for training the end-to-end human trajectory model JOSH3R, its scale is already much larger than existing in-the-wild global human motion datasets EMDB2 [7] and SLOPER4D [14] with about 100,000 annotated frames. This further shows that the small scale of existing datasets can limit the learning of end-to-end global human motion models from image inputs and the high potential of learning such models with pseudo-labels from web data. Some visualizations of the pseudo labels are depicted in Fig. 6, showing the high diversity of pedestrian movements and scene context from web videos.

C. Full Comparison on EMDB

As EMDB [7] is the most widely used dataset for evaluating global human motion estimation, we perform an extensive comparison with other methods in Tab. 5. It can be shown that JOSH outperforms all the state-of-the-art methods, and JOSH3R still achieves comparable results on EMDB. As the image resolution, scene background, and human trajectory are all very different from the annotated web videos used to train JOSH3R, it has degraded performance compared to the SLOPER4D [14] dataset, which has similar urban environments and human motion to the ones shown in Fig. 6. As JOSH3R is the first end-to-end model for estimating global human trajectory from monocular videos, we believe training it with more diverse data could lead to a more generalized model and bridge the domain gap.



Figure 6. **Web videos annotated by JOSH.** The first row shows the initial frame of the sequence with pedestrians walking in urban scenes. The second row shows pseudo-labels of the global human motion predicted by JOSH by projecting the future motion to the initial frame.

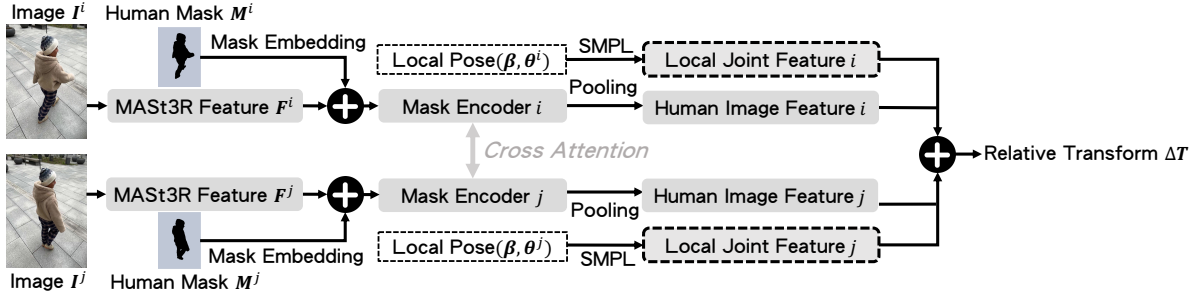


Figure 7. **Human trajectory head of JOSH3R.**

D. Ablation Studies on JOSH3R

A more detailed architecture of the human trajectory head of JOSH3R is shown in Fig. 7. The human trajectory head follows the siamese network design similar to MAST3R [13]. It takes the feature maps F^i, F^j after the frozen MAST3R encoder and decoder layers, the human masks M^i, M^j from a tracking model [34], and the optional human local pose parameters $\theta^i, \theta^j, \beta$ from a human mesh recovery model [37] as inputs. To encode the human subject’s information, the human trajectory head first adds the feature maps with a learnable mask embedding m on the human region, $F = F + (1 - M) \odot m$, to make the model aware of the 2D position of the human subject. It then passes the new feature maps with a mask encoder module to encode the human feature with a transformer decoder layer and a pooling layer on the masked region. The obtained human image features are finally concatenated with the optional human local joint features from the local 3D position of the SMPL body joints for both images. We use a simple MLP head to regress the final relative transformation ΔT . We analyze the effect of different components of JOSH3R with ablation studies in Tab. 6. We find that predicting the relative human transformation instead of the absolute human transformation (-Rel. Trans.) can benefit model learning as the output is not dependent on the current camera pose. Also, the optional local joint features (-Joint Feat.) can provide motion cues in addition to the human image features and improve accuracy. Finally, data augmentation (-D.A.) is important to address the scarcity of labels and learn a more generalized model.

Variants	SLOPER4D			
	WA-MPJPE ₁₀₀	W-MPJPE ₁₀₀	RTE%	ATE
-Rel. Trans.	559.5	1804.3	12.3	67.0
-Joint Feat.	325.4	1306.1	11.4	62.5
-D.A.	296.2	1314.3	10.5	60.5
JOSH3R	271.1	1217.1	10.0	56.1

Table 6. **Ablation experiments of JOSH3R on SLOPER4D.** "-Rel. Trans." means we predict the human transformation in the camera coordinate instead of the relative transformation in the human coordinate. "-Joint Feat." means only use the human image features to predict the relative transform without the local joint features. "-D.A." means without data augmentation during training.